Carbon 162 (2020) 273–282

Contents lists available at ScienceDirect

Carbon

journal homepage: www.elsevier.com/locate/carbon

Graphene-coffee waste derived carbon composites as electrodes for optimized lithium ion capacitors

Juan Luis Gómez-Urbano [a, b], Gelines Moreno-Fernández [a], María Arnaiz [a, b], Jon Ajuria [a], Teófilo Rojo [a, b], Daniel Carriazo [a, c, *]

[a] Centre for Cooperative Research on Alternative Energies (CIC energiGUNE), Basque Research and Technology Alliance (BRTA), Alava Technology Park, Albert Einstein 48, 01510, Vitoria-Gasteiz, Spain
[b] Universidad Del País Vasco UPV/EHU, 48080, Bilbao, Spain
[c] IKERBASQUE, Basque Foundation for Science, 48013, Bilbao, Spain

ARTICLE INFO

Article history:
Received 5 December 2019
Received in revised form
27 January 2020
Accepted 17 February 2020
Available online 18 February 2020

ABSTRACT

Herein we report an easy, ecofriendly and cheap synthetic approach for the preparation of carbon composites from the pyrolysis and activation of coffee waste and graphene oxide, and their evaluation as potential electrodes for lithium ion capacitors (LICs). An exhaustive optimization of some important parameters such as particle size, electronic conductivity or mass loading has been done for the battery-type electrode; whereas the optimum combination of specific surface area and pore size distribution were also investigated for the capacitor-type electrode. Optimized electrodes allowed to go one step beyond the state-of-the-art of biowaste based dual carbon LICs in terms of energy, power and cyclability. Assembled LICs show values of 100 Wh kg^{-1}_{AM} at 9000 W kg^{-1}_{AM} and retain above 80% of the initial capacitance after 3000 cycles, which is enhanced to 15,000 cycles by decreasing the voltage window.

1. Introduction

The exponential increase on the energy demand undergone by our society in the last decades requires the development of advanced energy storage devices not only capable to store as much energy as possible, but also being formed by safe, environmentally friendly and cheap components. “Lithium ion batteries” (LIBs) have dominated the market of energy storage for portable and cord-less applications in the last three decades due to their high energy density, high cell voltage and low-self discharge [1]. Nevertheless, “electrical double layer capacitors” (EDLCs) are the preferred choice when high power densities are required. Moreover, in contrast with batteries, they offer reliability, showing almost unlimited lifespan, exceeding in some cases millions of cycles [2]. A third technology, known as “metal ion capacitors” or “hybrid capacitors”, integrate a battery-type electrode with a capacitor-type one in the same cell, combining advantages of both technologies and therefore filling the gap for a certain number of applications where moderate energy densities at high powers are demanded [3]. Among them, “lithium-ion capacitors” (LICs), first reported by Amattuci and co-workers [4], have gained considerable attention due to the synergistic effects achieved when merging LIB and EDLC technologies [5].

Carbonaceous materials have been widely used for energy storage applications —including LICs technology— due to their low-cost, abundancy, variety of allotropes and transformations, as well as superior physical/chemical stability [6,7]. It is remarkable that dual carbon LICs, in which both electrodes are based on carbonaceous materials, exhibit a much better long-term cycling stability than LICs containing metal insertion-type positive electrodes [8] or alloy-type negative electrodes [9]. Moreover, since the performance of LICs is closely related to the microstructure of carbons, several strategies have been explored for the preparation of advanced microstructured carbons (*e.g.* highly oriented rGO sponges [10], graphdiyne powder [11] or N-doped CNT/amorphous carbon [12]). However, in most of the cases the synthesis processes are time consuming, expensive and therefore difficult to scale up. Within this context, biomass derived carbons are a friendly alternative, usually prepared by simply thermally treating agricultural and forest biomass waste at high temperature. The resulting carbons showing high electrochemical activity, are promising materials to be used, either as positive or negative electrodes, in dual carbon

* Corresponding author. Centre for Cooperative Research on Alternative Energies (CIC energiGUNE), Basque Research and Technology Alliance (BRTA), Alava Technology Park, Albert Einstein 48, 01510, Vitoria-Gasteiz, Spain.
E-mail address: dcarriazo@cicenergigune.com (D. Carriazo).

https://doi.org/10.1016/j.carbon.2020.02.052

LICs [6,13]. However, owing to the different charge storage mechanisms that governs each type of electrode, an individual optimization needs to be carried out to meet their own requirements.

In order to improve the power performance in the battery-type electrode, in which lithium insertion occurs, several parameters need to be carefully optimized. Special attention needs to be paid to the carbon structure in order to reversibly accommodate a large quantity of lithium ions without plating any lithium. Formation of lithium dendrites can not only led to battery failure but can also result in severe safety hazard related to the spontaneous reaction of metallic lithium in contact with oxygen or water [14]. Furthermore, carbon particle size is a critical parameter for Li-insertion anodes. On one side, very large carbon particles can hinder Li^+ kinetics resulting in lower capacity values, especially at high current densities. On the other side, too small particles can result in extremely low coulombic efficiencies (CE) during the first cycle with a considerable irreversible loss of active material that is detrimental for practical applications [15]. Another key parameter is related to the conductivity and connectivity of the different carbon particles. In this sense, the addition of graphene can endow the electrode with mechanical stability, improved connectivity not only between particles but also with the current collector and with a 3D conducting network along the electrode to fasten electron mobility and transference [16].

Regarding to the improvement of the energy performance in the capacitor-type electrode, both chemistry and texture of the materials need to be optimized. Specially, textural properties should be carefully considered, since the electrochemical adsorption/desorption of charge is directly related to the available specific surface area (SSA) of the electrode. In this sense, carbonaceous materials (*i.e.* activated carbons (ACs)) with a large SSA and a suitable pore size distribution (PSD) are required in order to promote and facilitate the adsorption of a larger number of electrolyte ions on their surface and thus the double layer formation [17].

Within this context, we have synthesized tailored graphene-carbon composites obtained from the pyrolysis of coffee waste powder and graphene oxide (GO) to be used in both the negative and the positive electrode of a LIC. The impact of the physicochemical properties of the materials as well as their processing on the electrochemical performance of both electrodes were investigated. Finally, properly optimized mass balanced LIC full cell was assembled using the best electrodes in order to maximize the performance not only in terms of energy density but also in terms of power and cyclability.

2. Experimental

2.1. Synthesis

Coffee waste collected from used capsules of a well-known coffee company, and graphene oxide from Graphenea (4 mg ml^{-1}) were chosen as carbon precursor and graphene source, respectively. In a preliminary step, GO/coffee waste powdered composite was prepared by mixing 2.5 g of coffee waste with 40 ml of 2 mg ml^{-1} GO and vigorously stirred overnight. Then the suspension was freeze-dried for 3 days to yield the dry GO/coffee waste precursor.

Hard carbon (HC) graphene composites were obtained by heating the powdered GO/coffee waste mixture at 950 °C for 1 h under dynamic Ar atmosphere. The sample hereafter denoted as GOCAF was obtained after ball milling (Planetary mill PULVERISETTE 5) at 250 r.p.m. using a ball:carbon mass ratio of 1:30. Milling process (30 min) was repeated six times using resting time of 5 min between each repetition. For the sake of comparison an additional sample without GO, denoted as CAF, was also prepared.

Two different ACs were prepared starting from the GO/coffee waste precursor. The GO/coffee waste mixture was pre-carbonized at 400 °C in a furnace for 3 h under dynamic Ar atmosphere. Then carbon was grounded together with KOH in a mortar using two different C:KOH mass ratios: 1:4 (AC4) and 1:6 (AC6) and furtherly heated at 800 °C for 1 h under Ar atmosphere. The resulting materials were washed one time using a diluted solution of HCl and then several times with hot deionized water. Dry powder was obtained after freeze and freeze-drying the material.

2.2. Physicochemical characterization

Morphological characterization was performed by scanning electron microscopy (SEM) in a Quanta200 FEI (3 kV, 30 kV) microscope and by transmission electron microscopy (TEM) in a FEI - TECNAI G2 F20 S-TWIN microscope at an acceleration voltage of 200 kV and a spot size of 3. X-ray diffraction (XRD) patterns were registered for powdered samples in a Bruker D8 X-ray diffractometer; data were collected at 40 kV and 30 mA using CuKα radiation over 2θ within the range from 5 to 90° at steps of 0.02° and a residence time of 5 s. Raman spectra were recorded with a Renishaw spectrometer (Nanonics Multiview 2000) operating with an excitation wave-length of 532 nm. The spectra were acquired with 30 s of exposition time of the laser beam to the sample. Nitrogen adsorption/desorption isotherms were registered at −196 °C in an ASAP 2460 from micromeritics. The specific surface area values were calculated using the Brunauer–Emmett–Teller (BET) equation in the relative pressure range between 0.05 and 0.25 and the pore size distributions were calculated by the 2D-NLDFT model applied from the data of the adsorption branches using the SAIEUS software.

2.3. Electrochemical characterization

Hard carbon (both GOCAF and CAF) and activated carbon (both AC4 and AC6) electrodes were processed by mixing the active materials together with Super P C65 (Imerys Graphite & Carbon), and polyvinylidene fluoride (PVDF) in N-methyl-2-pyrrolidone (NMP) according to the 90:5:5 mass ratio. HC and AC NMP-based inks were coated on copper and aluminum foil, respectively, fixing a thickness of 150 μm and then the laminates were dried at 80 °C under vacuum overnight. Electrode discs of 11 mm in diameter were punched out and dried at 120 °C overnight under vacuum prior the cell assembly.

HC-based electrodes were preliminarily evaluated in a half-cell configuration in a two-electrode Swagelok-type cell and using a lithium disc as counter and reference electrode. Galvanostatic charge/discharge measurements were carried at different C rates (being 1C: 372 mAh g^{-1} according to the theoretical capacity of graphite) between 0.002 and 2.0 V *vs.* Li/Li^+. Electrochemical impedance spectroscopy (EIS) measurements were performed for the HC-based electrodes in the fully discharged state after 5 cycles of charge/discharge at 0.1C. EIS measurements were conducted in three-electrode cells over frequency ranges from 100 kHz to 1 mHz and the extracted data were fitted using Zview software.

AC-based electrodes were evaluated in half-cell configuration in a three-electrode Swagelok-type cell using an oversized Norit (Kuraray) disc as counter electrode and a lithium disc as reference electrode. Galvanostatic charge/discharge measurements and cyclic voltammetries (CVs) were carried between 1.5 and 4.2 V *vs.* Li/Li^+. AC-based electrodes were also evaluated as symmetric EDLCs using a two-electrode Swagelok-type cell. Galvanostatic charge/discharge and CV measurements for EDLCs were performed within the 0–2.7 V cell voltage range.

LICs were assembled using a pre-lithiated HC as battery-type

negative electrode *vs.* an AC as capacitive-type positive electrode in three-electrode Swagelok-type cell using metallic lithium as reference electrode. HC potential was set to 0.2 V *vs.* Li/Li^+ and AC was charged up to 4.2 V *vs.* Li/Li^+. Prior full cell assembly, HC electrode was pre-lithiated in a two-electrode cell using lithium metal disc as counter and reference electrode. The pre-lithiation process involved 5 charge/discharge cycles at 0.1C between 0.002 and 2.0 V *vs.* Li/Li^+, an then a slow discharge at 0.025C from 2.0 V to 0.2 V. Galvanostatic charge/discharge measurements for the LIC were performed within the 1.5–4.2 V cell voltage range at different current densities.

Whatman D-type glass fiber discs of 13 mm in diameter and 1 M $LiPF_6$ in 1:1 in volume of ethylene carbonate (EC) and dimethyl carbonate (DMC) were used as separator and electrolyte, respectively in all the measurements. Specific capacity and current density values were calculated with respect to the total mass of active material.

3. Results and discussion

3.1. Hard carbon characterization

As already mentioned, the power performance of LICs is limited by the performance of the battery-type electrode since it involves lithium insertion/extraction mechanism which leads to a much stronger decay of capacity at high current densities compared to the capacitive electrode. Thus, in order to enhance the performance at high current densities without compromising lifetime, it is of paramount importance to find the most appropriate balance between morphology, particle size and surface area of carbons [15].

SEM images registered for the coffee waste derived carbon just after its pyrolysis (Fig. S1) reveal that the material is formed by particles of about *ca.* 200 μm in size, which contains macropores in a honeycomb structure. The addition of GO does not significantly modify neither the structure nor the particle size of the samples as can be observed from the SEM images. Despite its low content (6 ± 1 wt%), reduced graphene oxide (rGO) sheets, product of the thermal reduction of graphene oxide, fully cover the surface of the macroporous carbon particles in a homogeneous way, creating a conductive network along the whole sample. Controlled ball milling treatment of both samples produce a significant decrease in the particle size to 2–5 μm as can be observed in Fig. 1a and b. The combination of a small particle size and the presence of a conductive rGO network may fasten Li^+ diffusion through the particles and increase electronic conductivity along the whole composite [18].

TEM images registered for CAF and GOCAF samples show the presence of irregular-shaped HC particles in both of the materials, which in the case of the GOCAF sample are embedded within the graphene sheets (Fig. S2).

Additional characterization was performed on these samples to assess the impact of GO on the physicochemical properties of the composite. Textural properties were investigated through gas adsorption. Nitrogen adsorption/desorption isotherms registered for both samples (CAF and GOCAF) are included in Fig. 1c. Both of them show a similar adsorption profile ascribed to type-III according to the IUPAC classification that corresponds to the adsorption in macroporous or non-porous materials. It is worth noticing that, despite the low amount of graphene within the

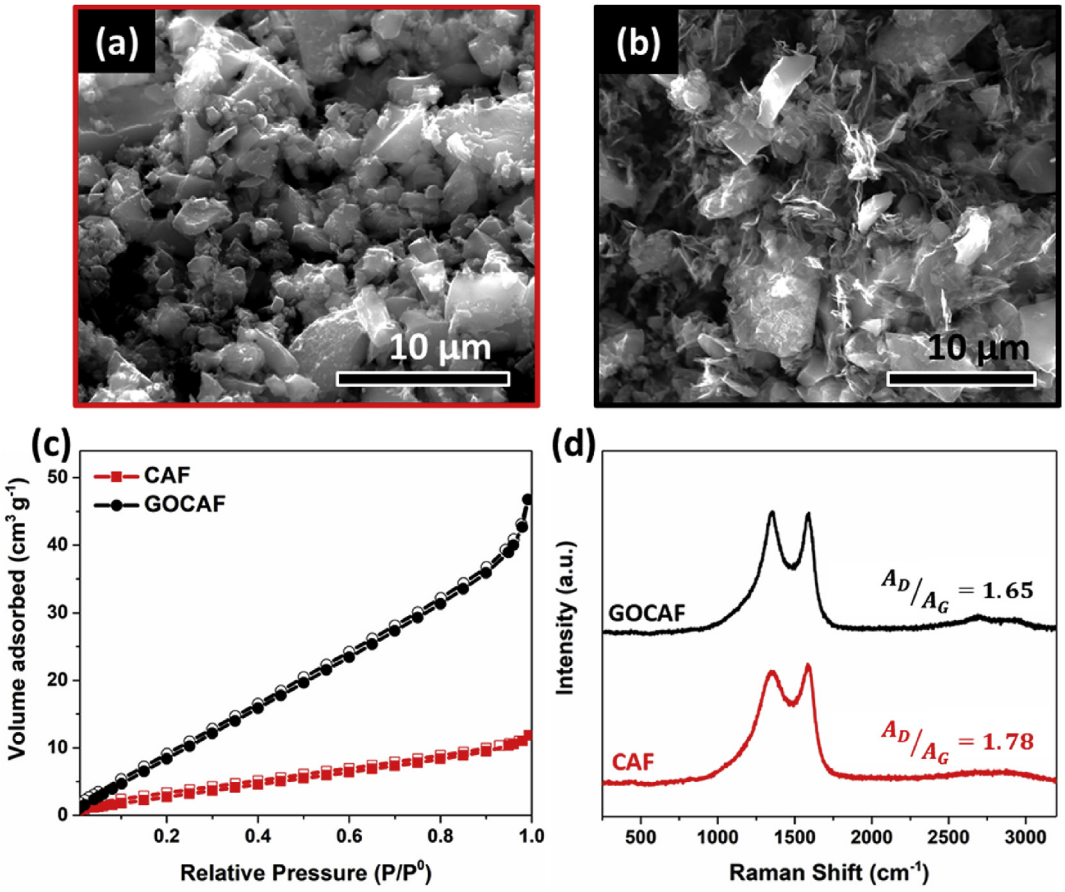

Fig. 1. SEM images of ball milled CAF **(a)** and GOCAF **(b)**. Nitrogen adsorption/desorption isotherms **(c)** and Raman spectra registered for the indicated samples **(d)**. (A colour version of this figure can be viewed online.)

sample, SSA is increased from 12 to 51 $m^2\ g^{-1}$ with the incorporation of graphene. Raman spectra registered for HCs are shown in Fig. 1d. Both of them show two broad peaks at *ca.* 1351 and 1599 cm^{-1}, assigned to the G and D bands of carbons, respectively. G-band is associated to the vibration of sp^2-type carbons while the D-band correspond to the dispersive defect induced vibrations [19]. From the ratio between peak integrated areas (A_D/A_G) values of 1.65 and 1.78 are calculated for GOCAF and CAF, respectively, indicating a lower concentration of defect and larger degree of graphitization in the graphene containing sample [20]. The XRD patterns measured for CAF and GOCAF are shown in Fig. S3. Both of them show two broad peaks assigned to the (002) and (100) diffraction planes of graphite, which are characteristic of amorphous/disordered carbons [21].

The electrochemical performance of CAF and GOCAF was evaluated at different C-rates (Fig. 2a). It is clearly observed that the incorporation of a low amount of graphene into the carbon composite produces a significant increase on the specific capacity in the whole range of current densities investigated. It should be also noted that this improvement is even more prominent at high current rates (Fig. S4a).

Galvanostatic charge/discharge curves registered for CAF and GOCAF samples are depicted in Fig. 2b and c. Both of them show sloping profiles without plateaus that are characteristic of Li^+ insertion in non-graphitic carbons [22]. It is worth to highlight that the capacity measured when charging process is stopped at 0.2 V *vs.* Li/Li^+ almost reaches the 70% of the full capacity, particularly when current densities over 1C are applied. This is important since it demonstrates that the material can operate under safe operation conditions while it provides high capacity values when formulated as the negative electrode in a LIC [5].

The GOCAF sample (Fig. 2c) shows outstanding gravimetric discharge capacity values of 398, 356, 305 and 195 mAh g^{-1} at current rates of 0.5C, 1C, 2C and 10C, respectively. The significant improvement measured in the graphene containing sample, whatever the current rate applied is, could be ascribed to a synergistic effect between rGO and the coffee waste derived carbon particles that enables fast insertion/extraction of lithium ions within the carbonaceous structure while graphene sheets creates a 3D conductive network that interconnects the whole sample enhancing its electronic conductivity [16]. Some representative capacity values reported for different carbons obtained from the pyrolysis of biowastes when tested as anodes for LIBs are summarized and compared with these results in Table 1. Besides, it can be observed that the incorporation of graphene does not strongly impact on the first cycle coulombic efficiency (Fig. S5), and values of 50 and 52% are obtained for the GOCAF and CAF samples, respectively. This could be ascribed to the low content of rGO in this sample (6 ± 1 wt%) which it is proved to be enough to increase the capacity and boost the rate capability compared to the CAF sample, but does not significantly increase the irreversible decomposition of the electrolyte and the solid electrolyte interphase formation on the surface of the particles [15].

The improved performance found for the graphene containing sample was further studied by EIS measurements (Fig. S6). Charge transfer resistance (R_{CT}), associated with the resistance of the electrochemical process, is reduced when graphene is incorporated into the sample (Table S1). Additional information about the EIS data and fitting values is included in the supporting information file.

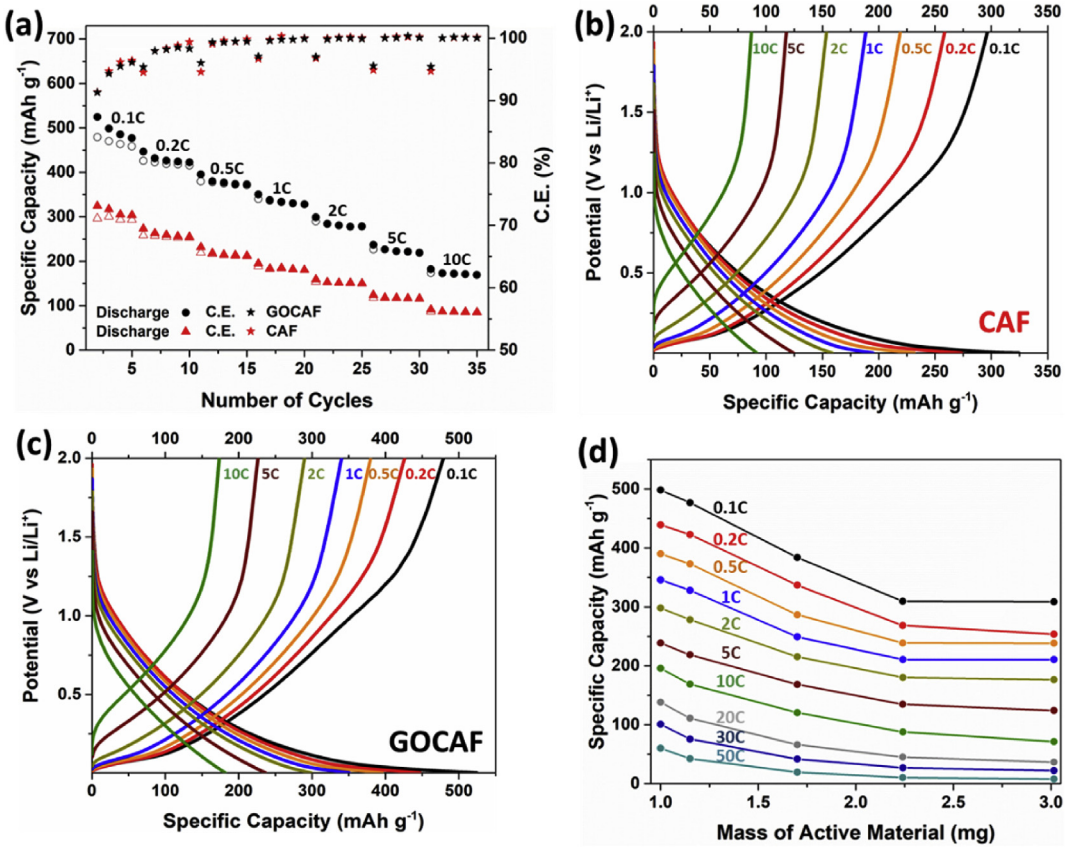

Fig. 2. Electrochemical characterization of Hard Carbon materials including, scan rate comparing CAF and GOCAF **(a),** Galvanostatic charge/discharge curves for CAF **(b)** and GOCAF **(c)** samples, and influence of active mass over specific capacity at different C rates for GOCAF sample **(d)**. (A colour version of this figure can be viewed online.)

Table 1
Electrochemical performance of some representative biomass waste derived carbons as negative electrodes for Li-ion energy storage systems.

Active material	Electrolyte	Current Density (mA g^{-1})	Capacity (mAh g^{-1})	Reference
Coffee waste derived carbon	$LiPF_6$ in EC:DEC	100	360	[26]
Olive pits derived carbon	$LiPF_6$ in EC:DMC	186 (0.5C)	230	[27]
Wheat straw derived carbon	$LiPF_6$ in EC:DMC	186 (0.5C)	250	[28]
Green-Tea derived carbon	$LiPF_6$ in EC:DMC	200	352	[29]
Loofah derived carbon	$LiPF_6$ in EC:DMC	200	346	[30]
rGO-coffee waste derived carbon (GOCAF)	**$LiPF_6$ in EC:DMC**	**186 (0.5 C)**	**398**	**This work**
Coffee waste derived carbon (CAF)	**$LiPF_6$ in EC:DMC**	**186 (0.5 C)**	**225**	**This work**

As it is generally known, the mass of electrodes plays a critical role in the electrochemical performance of the cell, and this is especially relevant at high current rates [23,24]. Within this context the performance of GOCAF was evaluated at different C-rates using different mass loadings as represented in Fig. 2d. This information is required to properly balance the gravimetric capacity in a final LIC. The impact of that mass loading of GOCAF on its electrochemical properties was studied in the mass range between 1 and 3 mg (0.9 and 2.8 mg cm^{-2}). As expected, the largest capacity values are obtained for the lowest mass loading whatever the C-rate applied. The specific capacity decreases progressively as the active mass increases from 1 to 2.2 mg and no significant differences are observed when moving from 2.2 to 3 mg. This behavior could be related to the progressive increase of the electrode resistance as the electrode is thickened, and to the negligible contribution of the external particles in the capacity output [25]. It should also be noted that the capacity loss when increasing the active mass from 1 to 3 mg is more prominent at high current rates (Fig. S4b), raising from 40% at 0.1C to 90% at 50C. Although it is not in the scope of the study, additional data regarding the influence of particle size over the electrochemical performance of Li-ion anodes are included in Fig. S7.

3.2. Activated carbon characterization

ACs are the preferred choice for positive electrodes in LICs. Herein, GO-coffee waste was chosen as precursor and KOH as activating agent for the preparation of the capacitor-type positive electrode. A pre-carbonization step was done at 400 °C and two different KOH activating ratios were explored (1:4 and 1:6 corresponding to AC4 and AC6, respectively).

SEM images of AC6 before and after the activation with KOH are shown in Fig. 3a and b, respectively. This sample is formed by carbon particles of approximately 5 μm in size that appears

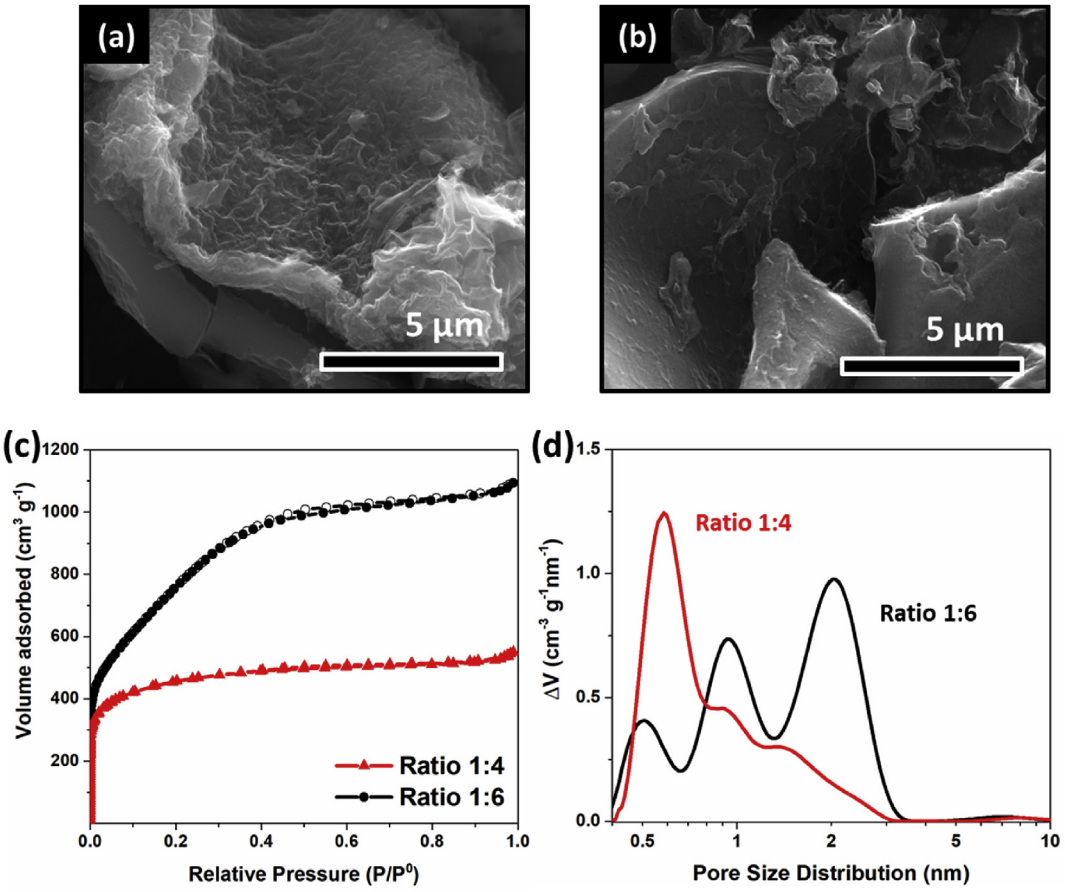

Fig. 3. SEM images of Activated Carbon ratio 1:6 (AC6) after **(a)** and before **(b)** KOH activation process and nitrogen adsorption/desorption isotherms **(c)** and resultant pore size distribution **(d)** for noted KOH activated carbons. (A colour version of this figure can be viewed online.)

homogeneously coated with rGO sheets in both of the samples. From these images no significant microscopic differences are observed between the activated and non-activated samples. Similar morphology is observed (see Fig. S8) for the sample activated using a lower amount of KOH (AC4).

Textural properties of these ACs were investigated by nitrogen adsorption/desorption at −196 °C (Fig. 3c). Isotherm registered on the AC4 sample can be indexed into type-I, which corresponds to microporous carbons, while AC6 exhibits a profile in between type-I and II, characteristic of samples containing a combination of both micropores and mesopores. The slight increase on nitrogen adsorption observed at high relative pressures, near the saturation point, reveals the presence of interparticle voids in both samples [31]. BET specific surface area values calculated for AC4 and AC6 are 1650 and 2350 $m^2\ g^{-1}$, respectively, pointing out the significant surface increase on the AC6 sample as consequence of its larger activating agent ratio [32]. PSD calculated from the isotherms of these two ACs are reported in Fig. 3d. This plot clearly shows that increasing the amount of KOH up to 6 produces an enlargement of the pore size as consequence of the collapse of contiguous small micropores giving rise to pores ranging from 1 to 2 nm [33].

The electrochemical performance of ACs was firstly investigated in the potential range of 1.5–4.2 V *vs.* Li/Li^+ in a three-electrode Swagelok-type cell using $LiPF_6$ in EC:DMC as electrolyte and an oversized electrode made from Norit (Kuraray) carbon as counter. Under these operating conditions, CV curves registered for AC6 at different sweep rates, show typical rectangular shaped profiles characteristic of capacitive charge storage mechanism. It is worth mentioning the high specific capacitance and low resistance measured in this sample even at high sweep rates. CV curves registered for the AC4 (Fig. S9a) show similar rectangular shape but lower specific capacitance (Fig. S9b). Evolution of specific capacitance (capacity) for both ACs (AC4 and AC6) was measured from the galvanostatic discharge branches at different current rates (Fig. 4b). Larger specific capacitances are measured for the AC6 sample in the whole current density range, which is surely ascribed to its larger SSA and wider porosity than those measured for the AC4 [17]. Specifically, more than 200 $F\ g^{-1}$ (150 $mAh\ g^{-1}$) are obtained at a current density of 0.25 $A\ g^{-1}$ while *ca.* 112 $F\ g^{-1}$ (84 $mAh\ g^{-1}$) are retained when increasing the current density to 10 $A\ g^{-1}$.

The good capacitive performance of AC6 carbon is furtherly confirmed when it is tested in a symmetric EDLC cell using $LiPF_6$ in EC:DMC as organic electrolyte in a voltage window of 0–2.7 V (Fig. 4c and d and Fig. S10). Some values reported recently for representative ACs obtained by the pyrolysis of different biowastes are summarized in Table 2. It is worth highlighting that under these circumstances, EDLC cells assembled using AC6 carbon outperform on capacitance and energy densities terms (*i.e.* 128 $F\ g^{-1}$ and 31 $Wh\ kg^{-1}$) those biowaste derived ACs reported in literature, either using conventional organic EDLC or battery-type electrolytes.

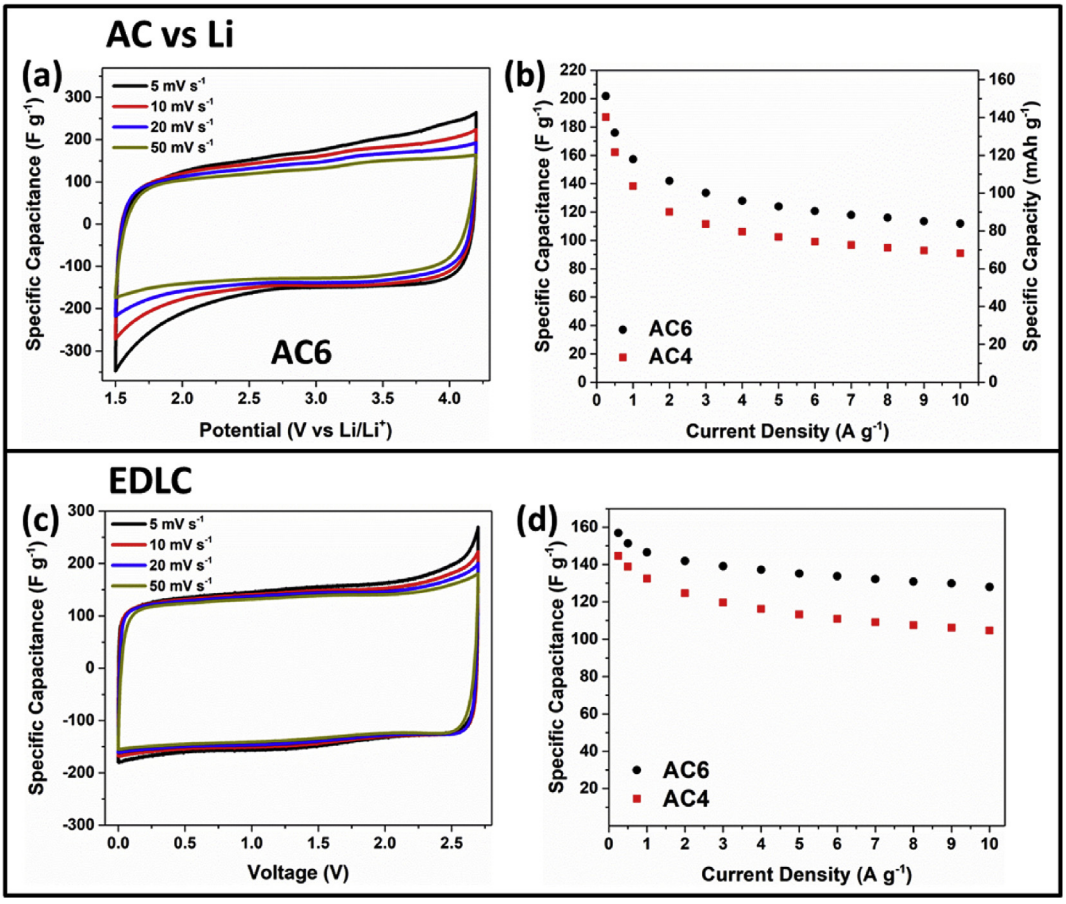

Fig. 4. CV curves of AC6 measured at different sweep rates in a three-electrode configuration system using lithium as reference and an oversized Norit electrode as counter **(a)** and specific capacitance evolution of AC6 and AC4 at different current rates in three-electrode configuration **(b)**. CV curves of AC6 measured at different sweep rates in an EDLC two-electrode configuration **(c)** and specific capacitance evolution of AC6 and AC4 in two-electrode configuration **(d)**. $LiPF_6$ in EC:DMC was the electrolyte used for all measurements. (A colour version of this figure can be viewed online.)

Table 2
Textural properties and electrochemical performance of some representative biowaste derived activated carbons used as electrodes in non-aqueous symmetric EDLC systems.

Material	Specific Surface area ($m^2\ g^{-1}$)	Electrolyte	Capacitance[a] ($F\ g^{-1}$)	Energy density[a] ($Wh\ kg^{-1}$)	Reference
KOH activated olive pits	2225	Et_4NBF_4/AN	90	22	[27]
$ZnCl_2$ activated coffee waste	1021	$TEABF_4$/AN	110	20	[34]
KOH activated coffee waste	1946	$BMIMBF_4$/AN	80	27	[35]
KOH activated human hair	1306	$LiPF_6$/EC:DEC	55	17	[36]
KOH activated indian cake rusk	1413	$LiPF_6$/EC:DMC	60	13	[37]
KOH activated coffee waste (AC6)	**2350**	**$LiPF_6$/EC:DMC**	**128**	**31**	**This work**

[a] Specific capacitance and gravimetric energy density values are calculated at the current density of 10 A g^{-1}

3.3. Lithium-ion capacitor performance

In view of their better performance, graphene-coffee waste derived hard carbon (GOCAF) and the AC within a 1:6 ratio (AC6) were selected as negative and positive electrode materials, respectively for the development of the final LIC. The individual evolution of the specific capacity values calculated for GOCAF and AC6 at different current rates using similar electrode masses are shown in Fig. 5a. It is clearly observed that the GOCAF exhibits a characteristic evolution of battery-type electrodes showing higher capacities at low current rates and a prominent capacity decay as the current rate is increased. In contrast, AC6 electrode shows lower capacitance at the beginning but with improved capacity retention, characteristic of capacitive materials. In order to fully balance the charge at approximately 10 A g^{-1} and keep the negative electrode slightly oversized to avoid its full utilization preventing lithium platting, a mass ratio of 1:1 was fixed for the final device [14]. As described in the experimental section, pre-lithiation of the GOCAF electrode was carried out before full cell assembly. Then, lithiated GOCAF was assembled together with AC6 in a three-electrode Swagelok cell using lithium metal as reference electrode. HC potential was set to 0.2 V *vs.* Li/Li^+ and AC was charged up to 4.2 V *vs.* Li/Li^+. The different potential ranges of the electrodes can efficiently enlarge the operating voltage window of the LIC, resulting in an enhanced energy density [8].

In Fig. 5b the galvanostatic charge/discharge curves measured at some representative current rates for the LIC are plotted. They show a linear voltage increase/decrease during charge and discharge, characteristic of the non-faradaic capacitive charge storage mechanism taking place with almost unappreciable ohmic drop up to 5 A g^{-1}, pointing out the low internal resistance of the LIC. To get insight on the contribution of each electrode into the full cell, individual galvanostatic charge/discharge profiles were monitored at representative current rates (Fig. 5c and d). It is observed that at

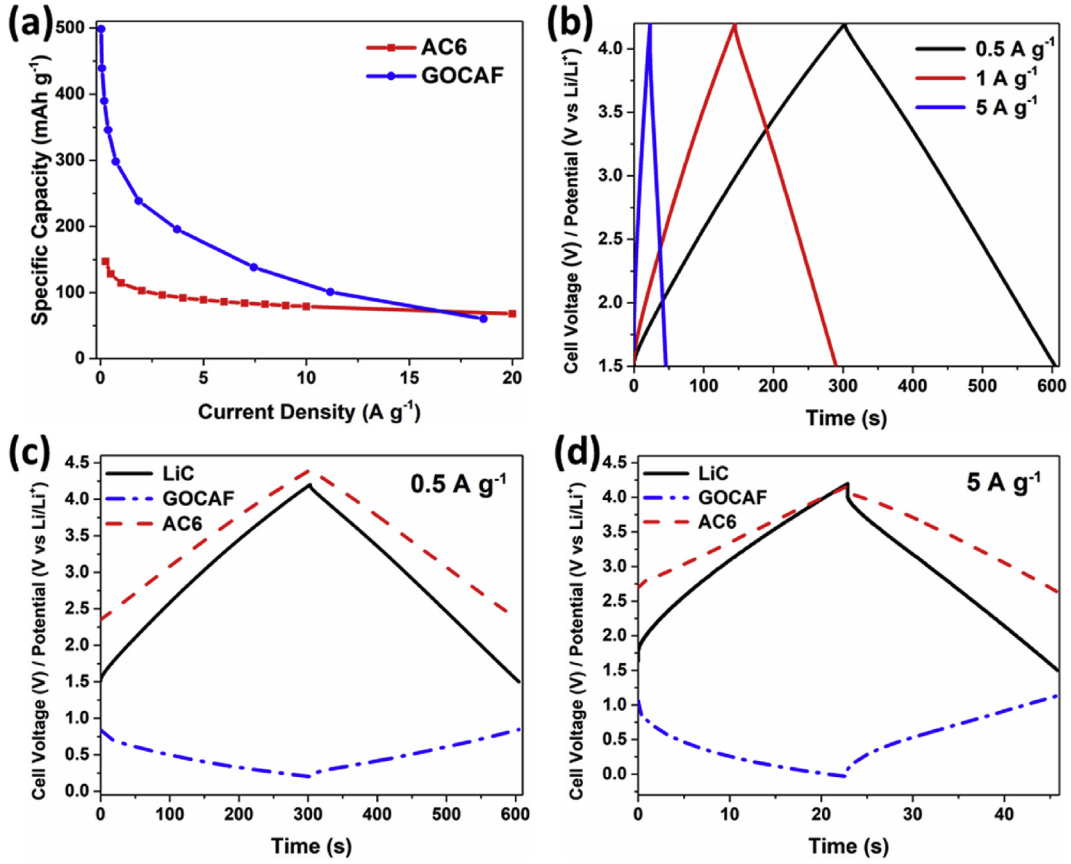

Fig. 5. Specific capacity evolution of AC6 and GOCAF at different current rates **(a)**, galvanostatic charge/discharge curve for the LIC at representative current rates **(b)**, and galvanostatic charge/discharge profiles registered at 0.5 **(c)** and 5 A g^{-1} **(d)** for the LIC (black), the negative electrode (blue) and the positive electrode (red). (A colour version of this figure can be viewed online.)

0.5 A g^{-1} (discharge time of 5 min), the positive electrode potential swings 2.1 V, while the negative electrode only fluctuates 0.6 V. When the current rate is increased to 5 A g^{-1}, the discharge time is reduced to *ca.* 25 s and the potential swing of the GOCAF-based negative electrode increases to *ca.* 1.0 V, while the potential swing of the AC decreases to 1.7 V. It is worth mentioning that even at 5 A g^{-1}, no lithium platting is observed, ensuring a safe operation of the cell. When current rate is increased over 8 A g^{-1} the potential of the GOCAF-based negative electrode reaches negative values (see Fig. S11), which can be risky not only affecting cyclability but also from a safety point of view. Taking this into account only values below 6 A g^{-1} were considered.

In Fig. 6a the energy-to-power ratio of the LIC calculated from the galvanostatic charge/discharge curves in the voltage range of 1.5–4.2 V is represented in a Ragone plot respect the total mass of active material and compared to the values measured for the AC6-based symmetric EDLC (0–2.7 V). Empty points of the curve represent energy/power values, for which the negative electrode reach negative potential values (from 6 A g^{-1} onwards).

It can be observed that for a similar power density, the LIC can deliver more than the triple of the energy corresponding to its EDLC counterpart, and still shows impressive energy retention (100 Wh kg^{-1}_{AM} at 9 kW kg^{-1}_{AM}). To the best of our knowledge, this LIC shows superior performance in terms of power compared to the biomass derived dual carbon based LICs reported so far in the state-of-the-art, as summarized in Table 3.

Fig. 6b shows the capacitance retention of the LIC tested within the 1.5–4.2 V cell voltage. As it can be observed, herein developed LIC reaches 80% of the initial capacitance after 3000 charge/discharge cycles at 5 A g^{-1} (discharge time less than 30 s). Nevertheless, if the operative voltage window is shortened to 2.0–4.0 V, even 15,000 cycles can be reached before the initial capacitance decays to 80% (Fig. S12). It is worth to highlight the good reversibility (ca. 99% coulombic efficiencies) maintained after long cycling regardless the voltage window.

4. Conclusions

The potential of ecofriendly and easy-scalable carbons derived from the pyrolysis and/or activation of coffee waste combined with graphene oxide and their application in lithium ion capacitors was demonstrated. It was shown that the optimization of different parameters such as particle size, electronic conductivity or activation degree in the corresponding materials have a great impact on the performance of the final electrodes. Specifically, it was found that the incorporation of graphene oxide into the hard carbon leads to a 40–70% increase of the capacity depending on the applied current rate. With regard to the activated carbon, AC6 showed specific

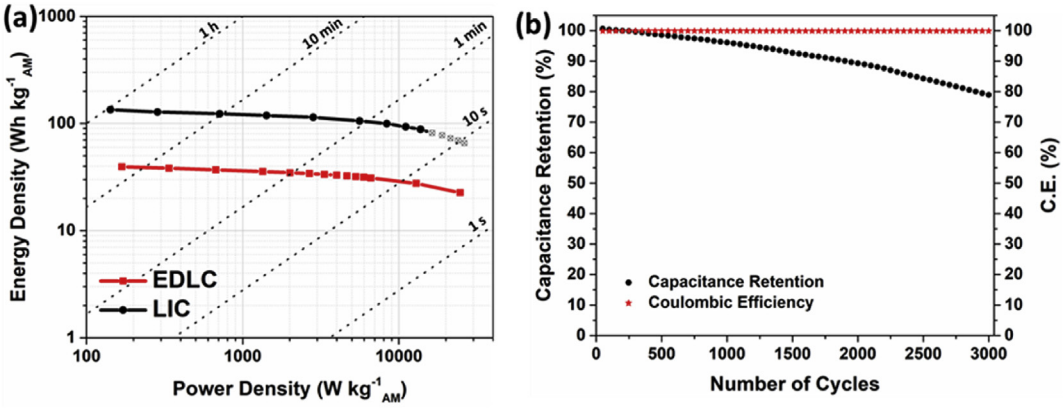

Fig. 6. Ragone plot comparing the gravimetric energy and power densities of the GOCAF/AC6-based LIC and the symmetric EDLC AC6-based symmetric EDLC **(a)**, and stability evolution of the GOCAF/AC6 LIC in the 1.5–4.2 V voltage range **(b)**. (A colour version of this figure can be viewed online.)

Table 3
Electrochemical performance of representative biowaste derived carbons as electrode for lithium-ion hybrid capacitors.

Positive electrode	SSA (m^2 g^{-1})	Positive electrode capacity[a] (mAh g^{-1})	Negative electrode	Negative electrode capacity (mAh g^{-1})	LIC Voltage Window	LIC Power Density[b] (kW kg^{-1})	Number of cycles (% Retention)	Ref
KOH activated olive pits	2225	120	Olive pits derived carbon	250 (0.5C)	1.5–4.2 V	2	5000 (70%)	[27]
KOH activated juliflora	2083	146	Juliflora derived carbon	400 (0.2 A g^{-1})	1.8–4.4 V	2	5000 (94%)	[38]
KOH activated juliflora	2448	95	Natural graphite	373 (0.1 A g^{-1})	2.0–4.0 V	3	7000 (80%)	[39]
$ZnCl_2$ activated coconut shell	1795	81	Coconut shell derived carbon	250 (0.1 A g^{-1})	1.7–4.2 V	3	8000 (83%)	[40]
KOH activated orange peel	1901	–	Graphite	–	2.0–4.0 V	0.5	1000 (80%)	[41]
$ZnCl_2$ activated teak wood	2108	70	Graphite	–	2.0–4.0 V	0.2	1000 (80%)	[42]
KOH activated natural sisal	3104	60	Mesocarbon microbeads	375 (0.1 A g^{-1})	2.0–4.0 V	1.28	1000 (93%)	[43]
KOH activated coffee waste	**2350**	**150**	**coffee waste derived carbon**	**398 (0.5 C)**	**1.5–4.2 V**	**9**	**3000 (80%)**	**This work**

[a] Positive electrode capacity corresponding to the current density of 0.1 A g^{-1}
[b] Power density values corresponding to energy density values of *ca.* 100 Wh kg^{-1}.

capacitance values of 200 F g^{-1} at low rates while 128 F g^{-1} are retained at 10 A g^{-1}. LICs assembled with these activated carbons and graphene-carbon composites show high energy density values of *ca.* 100 Wh kg^{-1}_{AM} at a high power density of 9000 W kg^{-1}_{AM}, accounting for more than three times the energy corresponding to the EDLC system. In addition, the device was able to reach 3000 cycles with an 80% retention of the initial capacitance when operating between 1.5 and 4.2 V, and 15,000 cycles when voltage window is fixed to 2.0–4.0 V.

Declaration of competing interest

The authors declare that they have no known competing financial interests or personal relationships that could have appeared to influence the work reported in this paper.

CRediT authorship contribution statement

Juan Luis Gómez-Urbano: Investigation, Methodology, Writing - original draft. **Gelines Moreno-Fernández:** Methodology, Writing - review & editing. **María Arnaiz:** Methodology, Writing - review & editing. **Jon Ajuria:** Validation, Writing - original draft. **Teófilo Rojo:** Supervision, Writing - review & editing. **Daniel Carriazo:** Conceptualization, Funding acquisition, Supervision, Writing - original draft.

Acknowledgments

The authors thank the European Union (Graphene Flagship, Core 2, Grant number 785219) and the Spanish Ministry of Science and Innovation (MICINN/FEDER) (RTI2018-096199-B-I00) for the financial support of this work. J. L. G. U. is very thankful to the Spanish Ministry of Education, Science and Universities (MICINN) for the FPU grant (16/03498). We are very grateful to María Jauregui and María Echeverría for their assistance with the XRD and TEM measurements, respectively. We also want to acknowledge the company GRAPHENEA for supplying the graphene oxide used in this work.

Appendix A. Supplementary data

Supplementary data to this article can be found online at https://doi.org/10.1016/j.carbon.2020.02.052.

References

[1] M. Li, J. Lu, Z. Chen, K. Amine, 30 Years of lithium-ion batteries, Adv. Mater. 30 (2018) 1800561, https://doi.org/10.1002/adma.201800561.
[2] A. González, E. Goikolea, J.A. Barrena, R. Mysyk, Review on supercapacitors: technologies and materials, Renew. Sustain. Energy Rev. 58 (2016) 1189–1206, https://doi.org/10.1016/j.rser.2015.12.249.
[3] H. Wang, C. Zhu, D. Chao, Q. Yan, H.J. Fan, Nonaqueous hybrid lithium-ion and sodium-ion capacitors, Adv. Mater. 29 (2017) 1702093, https://doi.org/10.1002/adma.201702093.
[4] G.G. Amatucci, F. Badway, A. Du Pasquier, T. Zheng, An asymmetric hybrid nonaqueous energy storage cell, J. Electrochem. Soc. 148 (2001) A930, https://doi.org/10.1149/1.1383553.
[5] X. Sun, X. Zhang, W. Liu, K. Wang, C. Li, Z. Li, et al., Electrochemical performances and capacity fading behaviors of activated carbon/hard carbon lithium ion capacitor, Electrochim. Acta 235 (2017) 158–166, https://doi.org/10.1016/j.electacta.2017.03.110.
[6] X. Wang, L. Liu, Z. Niu, Carbon-based materials for lithium-ion capacitors, Mater. Chem. Front. 3 (2019) 1265–1279, https://doi.org/10.1039/C9QM00062C.
[7] G. Li, Z. Yang, Z. Yin, H. Guo, Z. Wang, G. Yan, et al., Non-aqueous dual-carbon lithium-ion capacitors: a review, J. Mater. Chem. A. 7 (2019) 15541–15563, https://doi.org/10.1039/C9TA01246J.
[8] V. Aravindan, J. Gnanaraj, Y.-S. Lee, S. Madhavi, Insertion-type electrodes for nonaqueous Li-ion capacitors, Chem. Rev. 114 (2014) 11619–11635, https://doi.org/10.1021/cr5000915.
[9] C. Han, H. Li, R. Shi, L. Xu, J. Li, F. Kang, et al., Nanostructured anode materials for non-aqueous lithium ion hybrid capacitors, Energy Environ. Mater. 1 (2018) 75–87, https://doi.org/10.1002/eem2.12009.
[10] W. Ahn, D.U. Lee, G. Li, K. Feng, X. Wang, A. Yu, et al., Highly oriented graphene sponge electrode for ultra high energy density lithium ion hybrid capacitors, ACS Appl. Mater. Interfaces 8 (2016) 25297–25305, https://doi.org/10.1021/acsami.6b08298.
[11] H. Du, H. Yang, C. Huang, J. He, H. Liu, Y. Li, Graphdiyne applied for lithium-ion capacitors displaying high power and energy densities, Nano Energy 22 (2016) 615–622, https://doi.org/10.1016/j.nanoen.2016.02.052.
[12] S.R. Sivakkumar, A.G. Pandolfo, Carbon nanotubes/amorphous carbon composites as high-power negative electrodes in lithium ion capacitors, J. Appl. Electrochem. 44 (2014) 105–113, https://doi.org/10.1007/s10800-013-0606-6.
[13] S. Natarajan, Y. Lee, V. Aravindan, Biomass-derived carbon materials as prospective electrodes for high-energy lithium- and sodium-ion capacitors, Chem. Asian J. 14 (2019) 936–951, https://doi.org/10.1002/asia.201900030.
[14] Q. Liu, C. Du, B. Shen, P. Zuo, X. Cheng, Y. Ma, et al., Understanding undesirable anode lithium plating issues in lithium-ion batteries, RSC Adv. 6 (2016) 88683–88700, https://doi.org/10.1039/C6RA19482F.
[15] K. Zaghib, F. Brochu, A. Guerfi, K. Kinoshita, Effect of particle size on lithium intercalation rates in natural graphite, J. Power Sources 103 (2001) 140–146, https://doi.org/10.1016/S0378-7753(01)00853-9.
[16] J. Ajuria, M. Zarrabeitia, M. Arnaiz, O. Urra, T. Rojo, E. Goikolea, Graphene as vehicle for ultrafast lithium ion capacitor development based on recycled olive pit derived carbons, J. Electrochem. Soc. 166 (2019) A2840–A2848, https://doi.org/10.1149/2.0361913jes.
[17] R. Härmas, R. Palm, M. Härmas, M. Pohl, H. Kurig, I. Tallo, et al., Influence of porosity parameters and electrolyte chemical composition on the power densities of non-aqueous and ionic liquid based supercapacitors, Electrochim. Acta 283 (2018) 931–948, https://doi.org/10.1016/j.electacta.2018.06.115.
[18] W. Luo, C. Bommier, Z. Jian, X. Li, R. Carter, S. Vail, et al., Low-surface-area hard carbon anode for Na-ion batteries via graphene oxide as a dehydration agent, ACS Appl. Mater. Interfaces 7 (2015) 2626–2631, https://doi.org/10.1021/am507679x.
[19] I. Childres, L.A. Jauregui, W. Park, H. Cao, Y.P. Chen, RAMAN SPECTROSCOPY OF GRAPHENE AND RELATED MATERIALS, (n.d.) 20.
[20] X. Chen, X. Deng, N.Y. Kim, Y. Wang, Y. Huang, L. Peng, et al., Graphitization of graphene oxide films under pressure, Carbon 132 (2018) 294–303, https://doi.org/10.1016/j.carbon.2018.02.049.
[21] X. Dou, Hard Carbon Anode Materials for Sodium-Ion Battery, (n.d.) 120.
[22] B.N. Loeffler, D. Bresser, S. Passerini, M. Copley, Secondary lithium-ion battery anodes: from first commercial batteries to recent research activities, Johns Matthey Technol. Rev. 59 (2015) 34–44, https://doi.org/10.1595/205651314X685824.
[23] Y. Lee, The effect of active material, conductive additives, and binder in a cathode composite electrode on battery performance, Energies 12 (2019) 658, https://doi.org/10.3390/en12040658.
[24] W. Mei, H. Chen, J. Sun, Q. Wang, The effect of electrode design parameters on battery performance and optimization of electrode thickness based on the electrochemical–thermal coupling model, Sustain. Energy Fuel. 3 (2019) 148–165, https://doi.org/10.1039/C8SE00503F.
[25] F. Béguin, F. Chevallier, C. Vix-Guterl, S. Saadallah, V. Bertagna, J.N. Rouzaud, et al., Correlation of the irreversible lithium capacity with the active surface area of modified carbons, Carbon 43 (2005) 2160–2167, https://doi.org/10.1016/j.carbon.2005.03.041.
[26] F. Luna-Lama, D. Rodríguez-Padrón, A.R. Puente-Santiago, M.J. Muñoz-Batista, A. Caballero, A.M. Balu, et al., Non-porous carbonaceous materials derived from coffee waste grounds as highly sustainable anodes for lithium-ion batteries, J. Clean. Prod. 207 (2019) 411–417, https://doi.org/10.1016/j.jclepro.2018.10.024.
[27] J. Ajuria, E. Redondo, M. Arnaiz, R. Mysyk, T. Rojo, E. Goikolea, Lithium and sodium ion capacitors with high energy and power densities based on carbons from recycled olive pits, J. Power Sources 359 (2017) 17–26, https://doi.org/10.1016/j.jpowsour.2017.04.107.
[28] P. Yan, F. Ai, C. Cao, Z. Luo, Hierarchically porous carbon derived from wheat straw for high rate lithium ion battery anodes, J. Mater. Sci. Mater. Electron. 30 (2019) 14120–14129, https://doi.org/10.1007/s10854-019-01778-z.
[29] S. Sekar, Y. Lee, D.Y. Kim, S. Lee, Substantial LIB anode performance of graphitic carbon nanoflakes derived from biomass green-tea waste, Nanomaterials 9 (2019) 871, https://doi.org/10.3390/nano9060871.
[30] H. Hou, C. Yu, X. Liu, Y. Yao, Q. Liao, Z. Dai, et al., Waste-loofah-derived carbon micro/nanoparticles for lithium ion battery anode, Surf. Innov. 6 (2018) 159–166, https://doi.org/10.1680/jsuin.17.00068.
[31] M. Enterría, C. Botas, J.L. Gómez-Urbano, B. Acebedo, J.M. López del Amo, D. Carriazo, et al., Pathways towards high performance Na–O_2 batteries: tailoring graphene aerogel cathode porosity & nanostructure, J. Mater. Chem. (2018), https://doi.org/10.1039/C8TA07273F.
[32] E. Redondo, J. Carretero-González, E. Goikolea, J. Ségalini, R. Mysyk, Effect of pore texture on performance of activated carbon supercapacitor electrodes derived from olive pits, Electrochim. Acta 160 (2015) 178–184, https://doi.org/10.1016/j.electacta.2015.02.006.
[33] A.C. Lua, T. Yang, Effect of activation temperature on the textural and chemical properties of potassium hydroxide activated carbon prepared from pistachio-nut shell, J. Colloid Interface Sci. 274 (2004) 594–601, https://doi.org/10.1016/

j.jcis.2003.10.001.
[34] T.E. Rufford, D. Hulicova-Jurcakova, E. Fiset, Z. Zhu, G.Q. Lu, Double-layer capacitance of waste coffee ground activated carbons in an organic electrolyte, Electrochem. Commun. 11 (2009) 974–977, https://doi.org/10.1016/j.elecom.2009.02.038.
[35] Y.S. Yun, M.H. Park, S.J. Hong, M.E. Lee, Y.W. Park, H.-J. Jin, Hierarchically porous carbon nanosheets from waste coffee grounds for supercapacitors, ACS Appl. Mater. Interfaces 7 (2015) 3684–3690, https://doi.org/10.1021/am5081919.
[36] W. Qian, F. Sun, Y. Xu, L. Qiu, C. Liu, S. Wang, et al., Human hair-derived carbon flakes for electrochemical supercapacitors, Energy Environ. Sci. 7 (2014) 379–386, https://doi.org/10.1039/C3EE43111H.
[37] T. Kesavan, T. Partheeban, M. Vivekanantha, M. Kundu, G. Maduraiveeran, M. Sasidharan, Hierarchical nanoporous activated carbon as potential electrode materials for high performance electrochemical supercapacitor, Microporous Mesoporous Mater. 274 (2019) 236–244, https://doi.org/10.1016/j.micromeso.2018.08.006.
[38] P. Sennu, N. Arun, S. Madhavi, V. Aravindan, Y.-S. Lee, All carbon based high energy lithium-ion capacitors from biomass: the role of crystallinity, J. Power Sources 414 (2019) 96–102, https://doi.org/10.1016/j.jpowsour.2018.12.089.
[39] P. Sennu, V. Aravindan, M. Ganesan, Y.-G. Lee, Y.-S. Lee, Biomass-derived electrode for next generation lithium-ion capacitors, ChemSusChem 9 (2016) 849–854, https://doi.org/10.1002/cssc.201501621.
[40] S. Jayaraman, A. Jain, M. Ulaganathan, E. Edison, M.P. Srinivasan, R. Balasubramanian, et al., Li-ion vs. Na-ion capacitors: a performance evaluation with coconut shell derived mesoporous carbon and natural plant based hard carbon, Chem. Eng. J. 316 (2017) 506–513, https://doi.org/10.1016/j.cej.2017.01.108.
[41] M. Maharjan, M. Ulaganathan, V. Aravindan, S. Sreejith, Q. Yan, S. Madhavi, et al., Fabrication of high energy Li-ion capacitors from orange peel derived porous carbon, ChemistrySelect 2 (2017) 5051–5058, https://doi.org/10.1002/slct.201700574.
[42] A. Jain, S. Jayaraman, M. Ulaganathan, R. Balasubramanian, V. Aravindan, M.P. Srinivasan, et al., Highly mesoporous carbon from Teak wood sawdust as prospective electrode for the construction of high energy Li-ion capacitors, Electrochim. Acta 228 (2017) 131–138, https://doi.org/10.1016/j.electacta.2017.01.060.
[43] Z. Yang, H. Guo, X. Li, Z. Wang, Z. Yan, Y. Wang, Natural sisal fibers derived hierarchical porous activated carbon as capacitive material in lithium ion capacitor, J. Power Sources 329 (2016) 339–346, https://doi.org/10.1016/j.jpowsour.2016.08.088.